




Synthesis, crystal structure, magnetic, spectroscopic, and theoretical investigations of two new nitronyl-nitroxide complexes

Cristian Andrei Spinu, Céline Pichon, Gabriela Ionita, Teodora Mocanu, Sergiu Calancea, Mihai Raduca, Jean-Pascal Sutter, Mihaela Hillebrand & Marius Andruh

To cite this article: Cristian Andrei Spinu, Céline Pichon, Gabriela Ionita, Teodora Mocanu, Sergiu Calancea, Mihai Raduca, Jean-Pascal Sutter, Mihaela Hillebrand & Marius Andruh (2021) Synthesis, crystal structure, magnetic, spectroscopic, and theoretical investigations of two new nitronyl-nitroxide complexes, Journal of Coordination Chemistry, 74:1-3, 279-293, DOI: [10.1080/00958972.2021.1871900](https://doi.org/10.1080/00958972.2021.1871900)

To link to this article: <https://doi.org/10.1080/00958972.2021.1871900>



View supplementary material 



Published online: 22 Jan 2021.



Submit your article to this journal 



Article views: 82





View related articles 



View Crossmark data 



Synthesis, crystal structure, magnetic, spectroscopic, and theoretical investigations of two new nitronyl-nitroxide complexes

Cristian Andrei Spinu^a, Céline Pichon^b, Gabriela Ionita^c, Teodora Mocanu^{a,c},
Sergiu Calancea^{a,d}, Mihai Raduca^a, Jean-Pascal Sutter^b , Mihaela Hillebrand^e
and Marius Andruh^a 

^aInorganic Chemistry Laboratory, Faculty of Chemistry, University of Bucharest, Bucharest, Romania;

^bLaboratoire de Chimie de Coordination du CNRS (LCC), Université de Toulouse, CNRS, Toulouse, France; ^c“Ilie Murgulescu” Institute of Physical Chemistry, Romanian Academy, Bucharest, Romania;

^dFaculty of Chemistry and Chemical Technology, Moldova State University, Chisinau, Moldova;

^ePhysical Chemistry Department, Faculty of Chemistry, University of Bucharest, Bucharest, Romania

ABSTRACT

Two mononuclear complexes $[(Et_3NH)[M(hfac)_2L]]$ ($M = Ni$, **1**; Zn , **2**) have been synthesized using a nitronyl-nitroxide radical substituted nitrophenol, that is 2-(2-hydroxy-3-methoxy-5-nitrophenyl)-4,4,5,5-tetramethyl-4,5-dihydro-1H-imidazol-3-oxide-1-oxyl, HL, as a proligand. The crystal structures of **1** and **2** have been solved and indicate an octahedral coordination geometry of the metal ions. The magnetic behavior for **1** is characterized by a strong anti-ferromagnetic metal–radical interaction ($J = -351 \pm 1 \text{ cm}^{-1}$; $H = -JS_{Ni}S_{Rad}$). This exchange interaction was rationalized by DFT calculations. The EPR spectra recorded in both solution and solid state at 120 K confirm the $S = 1/2$ ground state for **1**.







ARTICLE HISTORY

Received 10 October 2020

Accepted 2 January 2021

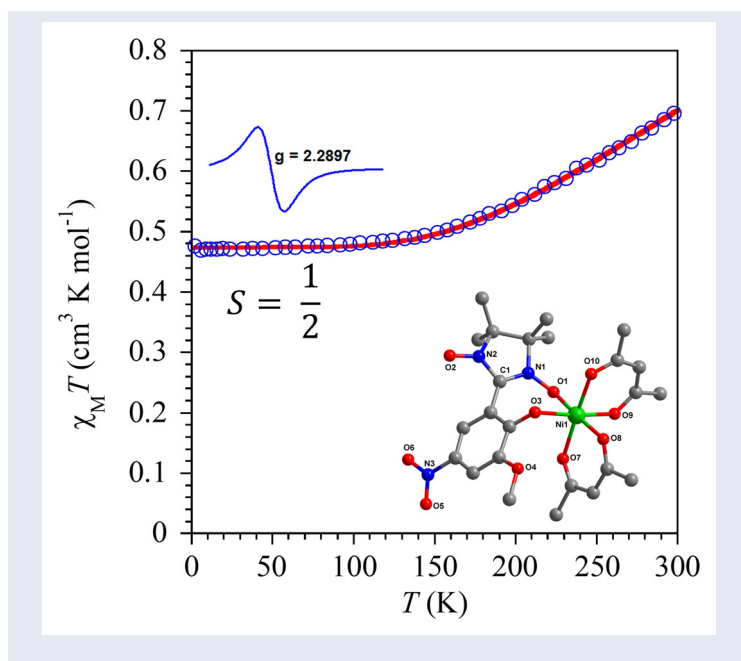
KEYWORDS

Nickel complexes; nitronyl-nitroxide ligands; magnetic properties; EPR spectra; zinc complexes

CONTACT Marius Andruh  marius.andruh@dnt.ro  Inorganic Chemistry Laboratory, Faculty of Chemistry, University of Bucharest, Str. Dumbrava Rosie 23, Bucharest, 020464, Romania; Mihaela Hillebrand  mihaela.hillebrand@gmail.com  Physical Chemistry Department, Faculty of Chemistry, University of Bucharest, Bd. Elisabeta 4-12, 030018-Bucharest, Romania; Jean-Pascal Sutter  sutter@lcc-toulouse.fr  Laboratoire de Chimie de Coordination du CNRS (LCC), Université de Toulouse, CNRS, Toulouse, France
This article has been republished with minor changes. These changes do not impact the academic content of the article.

 Supplemental data for this article is available online at <https://doi.org/10.1080/00958972.2021.1871900>

© 2021 Informa UK Limited, trading as Taylor & Francis Group

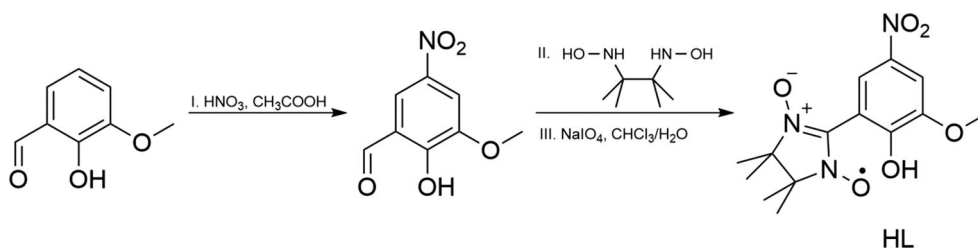


1. Introduction

A large family of molecular magnetic materials consists of heterospin complexes generated by *d* or *f* metal ions and paramagnetic organic radicals as ligands [1]. The most popular radicals are the nitronyl-nitroxides, which are readily obtained, starting from aldehydes, following or adapting Ullman's synthetic approach [2]. The rich diversity of nitronyl-nitroxide ligands arises from the availability of a very large number of mono- and polyaldehydes, as well as from the possibility to decorate the nitronyl-nitroxide platform with other coordinating groups (pre-existing in the starting aldehydes), which play an important role on the nuclearities and spin topologies of the resulting systems [3]. The family of magnetic materials constructed using paramagnetic organic ligands has been recently extended with polynuclear complexes containing two different metal ions, both paramagnetic [4]. Most of these heterotriscipin complexes contain 3*d* and 4*f* metal ions.

The exchange interactions between 2*p* radicals and paramagnetic metal ions vary between large limits, from strong antiferromagnetic to strong ferromagnetic couplings [1, 3], and usually the 2*p*-*nd* couplings are stronger than those involving lanthanides. Magnetostructural studies highlight the factors influencing the nature and strength of the exchange interactions [1]. The geometric parameters, at the level of aminoxyl-metal bond, influence the orientation of the magnetic orbitals, π^* (radical) and *d* or *f*, and, consequently, their overlap or orthogonality.

Surprisingly, in spite of their simplicity and popularity in coordination chemistry, *o*-vanillin [5] and its substituted derivatives have rarely been employed as precursors for nitronyl-nitroxide ligands. To the best of our knowledge, there is only one report on



Scheme 1. Synthesis of the paramagnetic ligand.

the synthesis of the nitronyl-nitroxide obtained from *o*-vanillin [6], but this radical has never been employed as a ligand. This might be related to the poor yield of the synthesis of the radical derived from *o*-vanillin. A more convenient method consists in employment of derivatives that contain a substituent in *para* position with respect to the phenolic group, preventing the formation of by-products during the oxidation step with sodium periodate. The nitro-derivative can be easily synthesized from *o*-vanillin and nitric acid and is subsequently transformed into the desired radical, HL (Scheme 1) [7]. In this article, we report the synthesis, crystal structure, and physical properties of two new mononuclear compounds, which contain L^- as a ligand, $(Et_3NH)[M(hfac)_2L]$ ($M = Ni, Zn$).

2. Experimental

2.1. General procedures

Syntheses of 2,3-dimethyl-2,3-dinitrobutane and 2-hydroxy-3-methoxy-5-nitrobenzaldehyde were performed according to reported procedures [8, 9]. All other reagents and solvents were commercially purchased and used without further purification, if not stated otherwise. IR spectra were recorded on a FTIR Bruker Tensor V-37 spectrophotometer (KBr pellets) from 4000 to 400 cm^{-1} . UV-Vis diffuse reflectance spectra were recorded on a JASCO V-670 spectrophotometer on undiluted samples from 200 to 1800 nm. Elemental analyses (C, H, and N) were performed on a EuroEA Elemental Analyzer. All nuclear magnetic resonance (^1H and ^{13}C NMR) measurements were recorded on a Bruker 500 MHz spectrometer at 25°C in CDCl_3 . X-ray powder diffraction measurements were carried out on a Proto AXRD Benchtop using $\text{Cu-K}\alpha$ radiation with a wavelength of 1.54059 \AA in the range $5\text{--}35^\circ$ (2θ). The metal ratio in the compound $[\text{Ni}_{0.2}\text{Zn}_{0.8}]$ was determined using element energy dispersive spectroscopy (EDS) (Smart Insight AMETEK), coupled with a Nova NanoSEM 630 Scanning Electron Microscope (FEI Company, Hillsboro, OR). The EDAX spectrum was acquired at an acceleration voltage of 18 kV, with a working distance of 5 mm and $30,000\times$ magnification.

EPR spectra were recorded with a JEOL FA 100 spectrometer equipped with a VT controller using the following setting: microwave power 1 mW, frequency 100 kHz, sweep field 2000 G, center field 3221.8 G, sweep time 1800 s, and modulation width 2 G.

The magnetic field calibration was performed with a DPPH (diphenylpicrylhydrazyl) standard marker, exhibiting a narrow EPR line at $g = 2.0036$. EPR spectra of zinc and nickel complexes and their mixture (molar ratio Ni/Zn 2:8) were recorded by filling a

Table 1. Crystallographic data, details of data collection, and structure refinement parameters for **1** and **2**.

Complex	1	2
Empirical formula	C ₃₀ H ₃₅ N ₄ NiO ₁₀ F ₁₂	C ₃₀ H ₃₅ N ₄ ZnO ₁₀ F ₁₂
Formula weight	898.33	904.99
Temperature (K)	293.15	293.15
Crystal system	Monoclinic	Monoclinic
Space group	<i>P</i> 2 ₁ / <i>c</i>	<i>P</i> 2 ₁ / <i>c</i>
<i>a</i> (Å)	20.2955(15)	20.4327(7)
<i>b</i> (Å)	9.6043(6)	9.5457(2)
<i>c</i> (Å)	21.5013(15)	21.5624(7)
α (°)	90	90
β (°)	110.349(5)	111.461(4)
γ (°)	90	90
Volume (Å ³)	3929.6(5)	3914.0(2)
<i>Z</i>	4	4
<i>D_c</i> (g/cm ³)	1.518	1.536
Absorption coefficient (mm ^{−1})	0.607	0.741
<i>F</i> (000)	1836.04	1844.0
Θ range for data collection (°)	1.93 to 24.999	2.03 to 30.783
Index ranges	−24 ≤ <i>h</i> ≤ 24, −11 ≤ <i>k</i> ≤ 11, −25 ≤ <i>l</i> ≤ 25	−25 ≤ <i>h</i> ≤ 26, −10 ≤ <i>k</i> ≤ 13, −26 ≤ <i>l</i> ≤ 27
Reflections collected	40888	39190
Independent reflections [<i>R</i> _{int}]	6936 [<i>R</i> _{int} = 0.1320]	9656 [<i>R</i> _{int} = 0.0337]
Completeness to Θ full (%)	100.0	100.0
Data / restraints / parameters	6936 / 18 / 642	9656 / 25 / 654
Goodness of fit on <i>F</i> ²	1.039	1.015
<i>R</i> ₁ , <i>wR</i> ₂ [<i>I</i> > 2 σ <i>I</i>]	0.0596, 0.1108	0.0378, 0.0984
<i>R</i> ₁ , <i>wR</i> ₂ (all data)	0.1414, 0.1476	0.0680, 0.1111
Largest diff. peak/hole (Å ³)	0.23/−0.34	0.28/−0.24

glass capillary that was placed in an EPR tube. For solution samples, the complexes or nitronyl-nitroxide radicals were dissolved in CH₂Cl₂; oxygen has been removed from solution by bubbling Ar gas. Frozen spectra were recorded at 120 K. The *a_N* values of nitronyl-nitroxide radical were obtained by simulation of experimental spectra using the Winsim program.

Magnetic measurements for **1** were carried out with a Quantum Design MPMS 5S SQUID magnetometer from 2 to 300 K. The crystalline powder of the complex was mixed with grease in a gelatin capsule. The temperature dependence of the magnetization was collected in an applied field of 1 kOe, and the isothermal field dependence of the magnetizations was collected up to 5 T. The molar susceptibility (χ_M) was corrected for sample holder, grease, and for the diamagnetic contribution of all the atoms by using Pascal's tables. Possible slow relaxation of the magnetization was examined by AC susceptibility collected in zero field and with applied fields.

2.2. X-Ray data collection and crystal structure refinement

Crystallographic data were collected on a STOE IPDS II diffractometer for **1** and on a Rigaku XtaLAB Synergy, single source at offset/far, HyPix diffractometer for **2** using a graphite-monochromated Mo K α radiation source ($\lambda = 0.71073$ Å). The structures were solved by direct methods and refined by full-matrix least squares techniques based on *F*². The non-H atoms were refined with anisotropic displacement parameters. Hydrogens were placed in fixed, idealized positions, and refined as rigidly bonded to

the corresponding atoms. Calculations were performed using SHELXT and SHELXL-2015 crystallographic software packages [10]. A summary of the crystallographic data and the structure refinement is given in Tables 1 and S1. CCDC reference numbers: 2032386 (**1**); 2032384 (**2**); 2032385 ($\text{Ni}_{0.2}\text{Zn}_{0.8}$).

2.3. Synthesis of 2,3-bis(hydroxylamino)-2,3-dimethylbutan

The synthesis of this ligand was adapted from a reported procedure [11]. A solution of HgCl_2 (1.028 g, 3.78 mmol) in 50 mL of water was added over strips of aluminum foil (1.534 g, 57.82 mmol). The mixture was stirred for 2 min after which the liquid was removed with a pipette. The amalgamated aluminum was cooled keeping it in a beaker immersed in an ice bath, and then a solution of 2,3-dimethyl-2,3-dinitrobutane (2 g, 11.36 mmol) in 60 mL of THF and 6 mL of H_2O was added sequentially. The reaction was left to evolve for 1 h, vigorously stirred at low temperature, followed by filtration on a pad of Celite which was washed with another 60 mL of THF. The solvents from the filtered solution were removed under vacuum to obtain a white precipitate. The precipitate was dissolved in 25 mL of CHCl_3 over which 25 mL of diethyl ether was added. The solution was left overnight in a freezer to form the product as a white crystalline powder, 0.555 g, yield 33%. The product was stored dried in a refrigerator. Anal. Calcd for $\text{C}_6\text{H}_{16}\text{N}_2\text{O}_2$ (%): C, 48.63; H, 10.88; N, 18.90. Found: C, 48.68; H, 10.90; N, 18.96. Selected IR peaks (cm^{-1}): 3368 (s), 3287 (s), 3252 (vs), 2988 (vs), 2943 (s), 1479 (m), 1452 (m), 1425 (m), 1404 (s), 1387 (s), 1375 (s), 1358 (m), 1261 (m), 1177 (m), 1146 (s), 1080 (m), 1036 (m), 989 (w), 951 (m), 932 (w), 905 (s), 853 (w), 791 (w), 690 (m), 609 (w), 494 (w), 441(w). ^1H -NMR (500.13 MHz, CDCl_3 , δ ppm): 1.19 (s, 12 H, CH_3 -); ^{13}C -NMR (125.77 MHz, CDCl_3 , δ ppm): 62.97 (CH_3 -C- CH_3), 20.81(CH_3 -).

2.4. Synthesis of 2-(2-hydroxy-3-methoxy-5-nitrophenyl)-4,4,5,5-tetramethyl-4,5-dihydro-1H-imidazol-3-oxide-1-oxyl (HL)

The synthesis of this ligand was devised and adapted from reported procedures [2, 7]. To a solution of 2,3-bis(hydroxylamino)-2,3-dimethylbutane (1.523 g, 10.288 mmol) in 50 mL of MeOH, another solution of 2-hydroxy-3-methoxy-5-nitrobenzaldehyde (1.843 g, 9.353 mmol) in 75 mL of MeOH was added. The mixture was refluxed for 4 h followed by evaporation of the solvent under vacuum. Over the yellow intermediate, 100 mL of CHCl_3 was added and the solution was ice-cooled, and then, a solution of NaIO_4 (2.002 g, 9.353 mmol) in 100 mL of water was added. The obtained biphasic system was vigorously stirred and the reaction left to evolve at 0°C for 15 min and then at 25°C for 45 min. The organic phase was isolated using a separatory funnel and dried with MgSO_4 . The solvent was evaporated under vacuum to obtain the crude blue product which was recrystallized four times from a mixture of CH_2Cl_2 :diethyl ether, 1:1 volumetric ratio, to obtain the pure blue product, 1.391 g, yield 46%. Anal. Calcd for $\text{C}_{14}\text{H}_{18}\text{N}_3\text{O}_6$ (%): C, 51.85; H, 5.59; N, 12.97. Found: C, 52.27; H, 5.41; N, 12.75. Selected IR peaks (cm^{-1}): 1581 (w), 1530 (m), 1462 (m), 1429 (m), 1394 (m), 1373 (w), 1350 (vs), 1258 (m), 1201 (w), 1163 (m), 1138 (w), 1105 (w), 1069 (w), 923 (w), 885 (w), 739 (m), 457 (m). UV-Vis (nm): 362, 571.

2.5. Synthesis of $(Et_3NH)[NiL(hfac)_2]$, **1**

$Ni(hfac)_2 \cdot 2H_2O$ (0.060 g, 0.1852 mmol) was dissolved in 15 mL of heptane and refluxed for 30 min. Then, after cooling the solution, another 15 mL of CH_2Cl_2 solution containing HL (0.094 g, 0.1852 mmol) and 1 drop of triethylamine was added. The solution was refluxed another 30 min, cooled and filtered. After allowing the solvent to slowly evaporate for three days, needle-shaped violet crystals of the product were obtained, 0.125 g, yield 75%. Anal. Calcd for $C_{30}H_{35}F_{12}N_4O_{10}Ni$ (%): C, 40.11; H, 3.93; N, 6.24. Found: C, 39.61; H, 4.13; N, 5.87. Selected IR peaks (cm^{-1}): 1657 (s), 1645 (s), 1600 (w), 1555 (m), 1524 (s), 1502 (s), 1396 (w), 1364 (m), 1310 (s), 1256 (vs), 1234 (m), 1204 (vs), 1148 (vs), 1097 (m), 1070 (w), 870 (w), 793 (m), 673 (m), 586 (w). UV-Vis (nm): 413, 571, 751, 1142.

2.6. Synthesis of $(Et_3NH)[ZnL(hfac)_2]$, **2**

$Zn(hfac)_2 \cdot 2H_2O$ (0.047 g, 0.0926 mmol) was dissolved in 7 mL of heptane and refluxed for 30 min. Then, after cooling the solution, another 7 mL of CH_2Cl_2 solution containing HL (0.030 g, 0.0926 mmol) and 1 drop of triethylamine was added. The solution was refluxed another 30 min, cooled and filtered. After allowing the solvent to slowly evaporate for three days, needle-shaped violet crystals of the product were obtained, 0.046 g, yield 55%. Anal. Calcd for $C_{30}H_{35}F_{12}N_4O_{10}Zn$ (%): C, 39.82; H, 3.90; N, 6.19. Found: C, 40.33; H, 3.80; N, 6.06. Selected IR peaks (cm^{-1}): 1663 (m), 1649 (s), 1601 (m), 1557 (m), 1528 (s), 1504 (s), 1399 (w), 1366 (m), 1331 (m), 1310 (s), 1286 (m), 1256 (vs), 1234 (m), 1204 (s), 1144 (vs), 1096 (m), 1071 (w), 869 (w), 795 (m), 765 (w), 746 (w), 669 (m), 583 (w). UV-Vis (nm): 424, 584.

The molecular alloy, $[Ni_{0.2}Zn_{0.8}(L(hfac)_2)]$, has been obtained by reacting the zinc and nickel salts in 1:4 molar ratio in the same experimental conditions described above for **1** and **2**. The powder X-ray diffractogram is similar to those recorded for **1** and **2** (Figure S3). The Ni:Zn molar ratio in the resulting alloy was confirmed by EDX measurements.

2.7. Computational details

The exchange coupling interaction was calculated by the DFT method using the Gaussian 09 program [12], considering two spin states, a low ($S = 1/2$ resulting from $S_{Ni} = 1$ and $S_{Rad} = -1/2$ spin states) and a high spin HS ($S = 3/2$ resulting from $S_{Ni} = 1$ and $S_{Rad} = 1/2$ spin states) one. The calculations were performed on the crystal geometry without further optimization. The energy of the low spin state, hereafter labeled as the broken symmetry (BS) state, was calculated by the fragment procedure as implemented in the Gaussian09 program and further checked for its stability. The calculations were performed using the basis set, TZVP [13], and three functionals, uB3LYP [14], uB3PW91 [15], and uM06 [16]. The EPR spectra of the Ni and Zn complexes were first calculated using the same theoretical model and the crystal geometry, but considering literature data [17], we have also used a new basis set recommended for EPR, TZVP/EPR-III, and a very simple one, 6-31 g*. Taking into account the results obtained by these models, the DCM solution spectra were

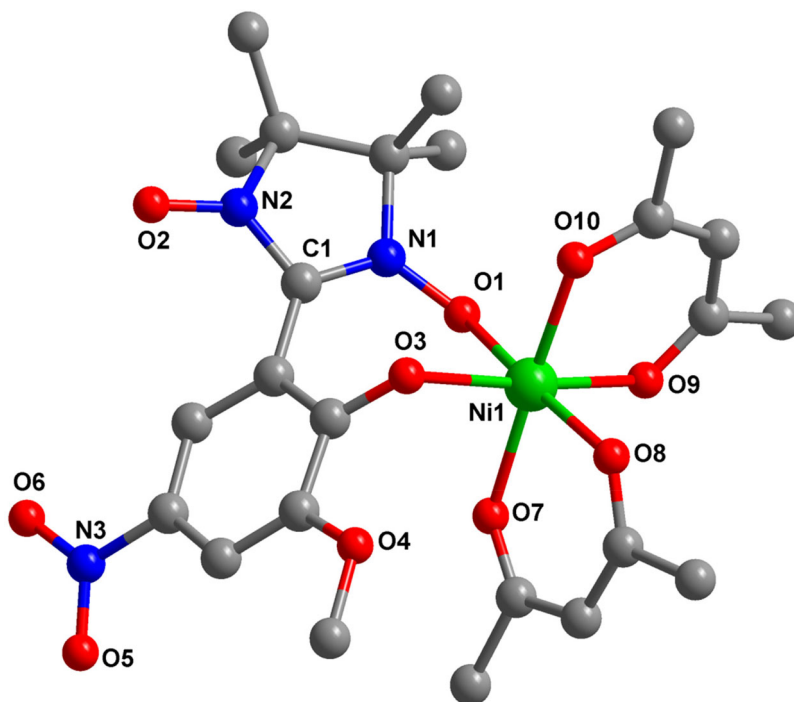


Figure 1. Molecular structure of the complex anion **1**, along with the atom numbering scheme. Hydrogen and fluorine atoms have been omitted for clarity.

calculated using only the TZVP and the 6-31 g* basis sets after the geometry optimization in the solvent.

3. Results and discussion

3.1. Description of the crystal structures

The new compounds, $(\text{Et}_3\text{NH})[\text{M}(\text{hfac})_2\text{L}]$ ($\text{M} = \text{Ni}$ **1**, Zn **2**), have been synthesized by reacting the metal precursors, $[\text{M}(\text{hfac})_2(\text{H}_2\text{O})_2]$, with the paramagnetic proligand, HL, in the presence of triethylamine, which was added for deprotonation of the phenolic group. The PXRD patterns for **1** and **2** confirm the purity of the crystalline phases (Figures S1 and S2). Since the two compounds are isostructural, only the crystal structure of **1** will be described in detail. Its crystal structure consists of anionic complex, $[\text{Ni}(\text{hfac})_2\text{L}]^-$ (Figure 1) and organic cation, Et_3NH^+ . The nickel ion has an octahedral geometry, coordinated by four oxygen atoms from the hfac^- ligands and two others from L^- (one phenoxido and one aminoxyl oxygen). The Ni–O oxygen distances vary between 2.008(4) and 2.072(4) Å. The N–O bond within the aminoxyl group coordinated to Ni^{II} (1.305(5) Å) is longer than the one within the uncoordinated NO group (1.266(5) Å). The complex is chiral and both enantiomers cocrystallize within the same crystal (Figure 2). The crystal structure of the complex anion in **2** is illustrated in Figure S4. Selected bond distances and angles for **1** and **2** are collected in Table 2. The diffuse reflectance spectra of the ligand and the two complexes are displayed in

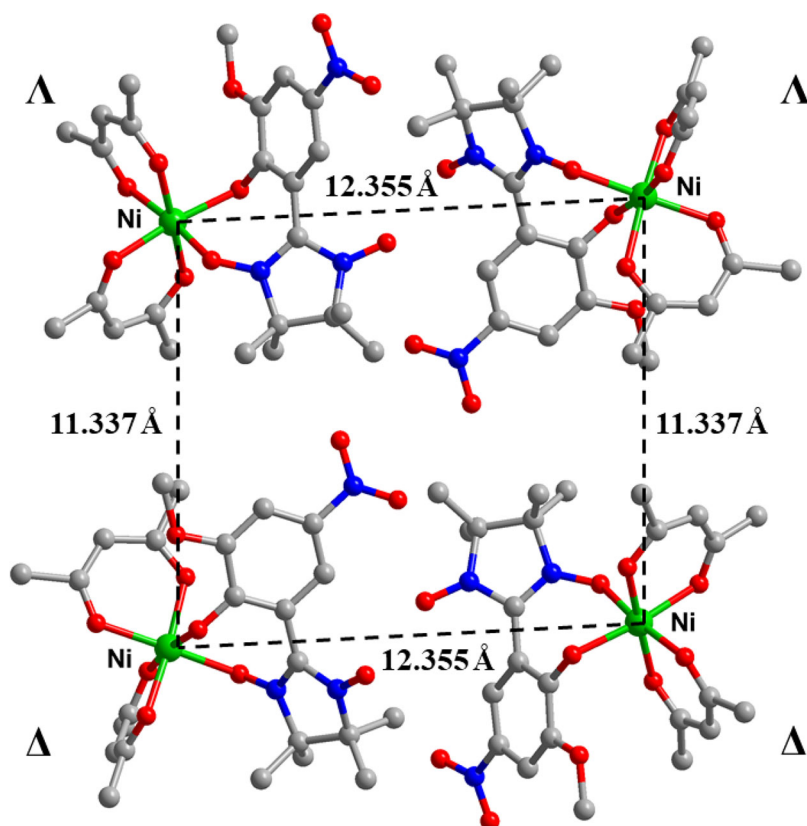


Figure 2. The packing diagram of 1 showing the closest distances between nickel metal ions and delta (Δ) or lambda (Λ) configurations of the metal centers.

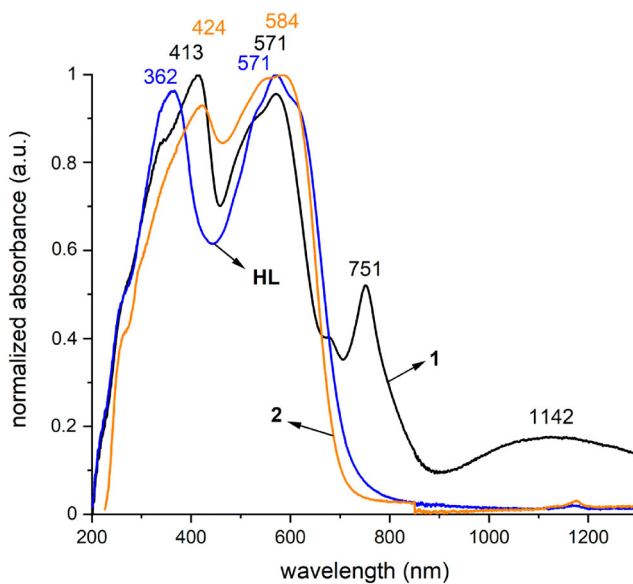


Figure 3. Diffuse reflectance spectra for HL, 1, and 2.

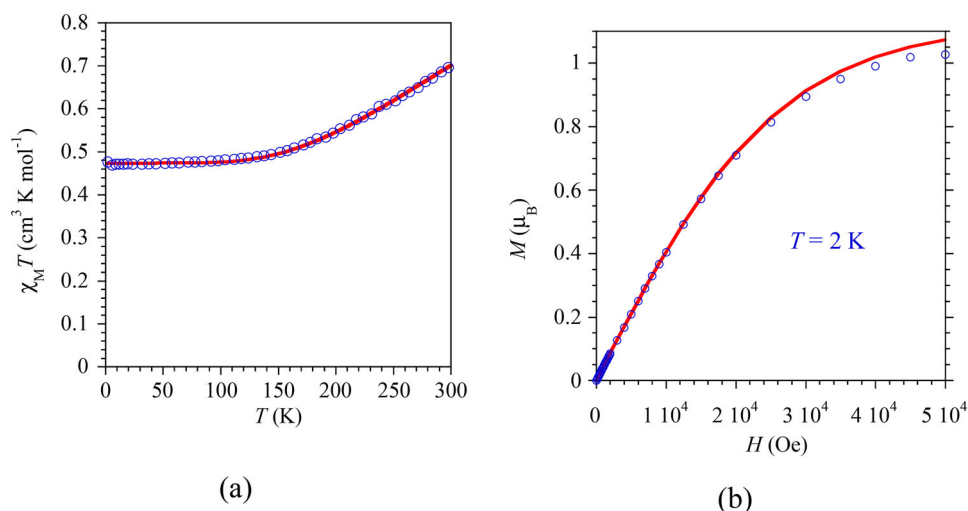


Figure 4. Magnetic behavior for **1**: experimental (O) and calculated (—) (a) temperature dependence of the $\chi_M T$ and (b) magnetization vs. field.

Table 2. Selected bond distances (Å) and angles (°) for **1** and **2**.

1		2	
Distances		Distances	
Ni1-O1	2.072(4)	Zn1-O1	2.204(2)
Ni1-O3	2.035(3)	Zn1-O3	2.035(1)
Ni1-O7	2.046(4)	Zn1-O7	2.095(2)
Ni1-O8	2.029(4)	Zn1-O8	2.089(2)
Ni1-O9	2.008(4)	Zn1-O9	2.051(2)
Ni1-O10	2.026(4)	Zn1-O10	2.090(2)
Angles		Angles	
O1-Ni1-O3	89.53(13)	O1-Zn1-O3	85.93(5)
O1-Ni1-O7	89.67(14)	O1-Zn1-O7	90.65(5)
O1-Ni1-O8	173.15(16)	O1-Zn1-O8	172.31(6)
O1-Ni1-O9	82.83(15)	O1-Zn1-O9	79.49(6)
O1-Ni1-O10	94.70(15)	O1-Zn1-O10	95.85(6)
O3-Ni1-O7	91.75(14)	O3-Zn1-O7	93.83(6)
O3-Ni1-O8	97.21(15)	O3-Zn1-O8	101.23(6)
O3-Ni1-O9	172.16(15)	O3-Zn1-O9	164.47(6)
O3-Ni1-O10	87.92(15)	O3-Zn1-O10	87.86(6)
O7-Ni1-O8	88.88(15)	O7-Zn1-O8	86.10(6)
O7-Ni1-O9	90.00(15)	O7-Zn1-O9	91.67(6)
O7-Ni1-O10	175.62(15)	O7-Zn1-O10	173.39(6)
O8-Ni1-O9	90.47(16)	O8-Zn1-O9	93.62(7)
O8-Ni1-O10	86.82(15)	O8-Zn1-O10	87.30(6)
O9-Ni1-O10	90.91(15)	O9-Zn1-O10	88.34(6)

Figure 3. Compound **1** shows, apart from the bands arising from the organic ligands, two other bands which are due to the $d-d$ transitions: ${}^3A_2 \rightarrow {}^3T_2$ (1122 nm) and ${}^3A_2 \rightarrow {}^3T_1$ (751 nm), assuming the O_h point group.

One single crystal from the $[\text{Ni}_{0.2}\text{Zn}_{0.8}]$ sample was measured, and the structure was refined with occupation factors 0.2 for Ni and 0.8 for Zn (Table S1), in agreement with the EDX data. The powder X-ray diffractogram for the alloy (Figure S3) is identical with those of **1** and **2**.

Table 3. Calculated J values (cm^{-1}) for **1**.

Functional	Equation (1)
uB3LYP	−400.53
uB3PW91	−398.23
uM06	−408.51

3.2. Magnetic properties of $(\text{Et}_3\text{NH})[\text{NiL}(\text{hfac})_2]$

The temperature dependence of the molar magnetic susceptibility, χ_M , for **1** has been investigated from 2 to 300 K, and the field dependence of the magnetization was recorded at 2 K. The $\chi_M T$ versus T and M versus H plots are presented in Figure 4. The value of $\chi_M T$ at 300 K is $0.70 \text{ cm}^3 \text{ mol}^{-1} \text{ K}$, much smaller than the expected $1.375 \text{ cm}^3 \text{ mol}^{-1} \text{ K}$ for the uncoupled $S = 1$ (Ni^{II}) and $S = 1/2$ (Rad). Moreover, reducing the temperature, $\chi_M T$ decreases to $0.475 \text{ cm}^3 \text{ mol}^{-1} \text{ K}$ at 120 K and below remains constant to 2 K. Such a behavior is indicative for a strong antiferromagnetic radical–Ni(II) interaction. The plateau reached below 150 K is the signature of a spin $S = 1/2$, resulting from the antiferromagnetic interaction between the spins $S = 1/2$ and 1. The resulting $S = 1/2$ ground state is further confirmed by the field dependence of the magnetization recorded at 2 K that tends to $1 \mu_B$ at 5 T. These magnetic data have been analyzed using the HDvV Hamiltonian: $\mathbf{H} = -J\mathbf{S}_{\text{Ni}}\mathbf{S}_{\text{Rad}}$. In order to avoid overparameterization, only a mean g parameter was considered (the local g parameters were accurately determined by EPR spectroscopy, *vide infra*). The best fit yielded $J = -351 \pm 1 \text{ cm}^{-1}$ and $g = 2.185 \pm 0.001$.

The nature of the exchange interactions (antiferro- and ferromagnetic) between nickel(II) and the aminoxyl group was subject of several magnetostructural correlation studies [18]. We recall here the most important conclusions, resulting from both experimental and theoretical investigations: (i) the coplanarity between the radical ring and the equatorial plane of the octahedral Ni^{II} ion favors a ferromagnetic coupling (the $d_{x^2-y^2}$ and π^* radical orbital are orthogonal, while the overlap with the d_{z^2} orbital is symmetry forbidden); (ii) the Ni–O–N–C dihedral angle as well as the Ni–O–N angle play a crucial role in overlap of the magnetic orbitals; (iii) large overlaps between the magnetic orbitals, and consequently, strong antiferromagnetic interactions are favored by M–O–N–C dihedral angles close to 90° and by Ni–O–N angles close to 120° . These geometrical parameters for **1** ($\text{Ni1–O1–N1} = 126.1(3)^\circ$, $\text{Ni1–O1–N1–C1} = 58.6(6)^\circ$) suggest that the coupling between the nickel(II) ion and the radical must be antiferromagnetic and quite strong, in line with the experimental value.

DFT calculations undertaken for **1** confirm the strong antiferromagnetic interaction between the paramagnetic centers, the ground state of the complex being the low spin state, that is the broken symmetry one.

Starting from the spin Hamiltonian previously mentioned, $\mathbf{H} = -J\mathbf{S}_{\text{Ni}}\mathbf{S}_{\text{Rad}}$, the J value was obtained using Equation (1) [19]:

$$J = (E_{\text{BS}} - E_{\text{HS}}) / (2S_{\text{Ni}}S_{\text{Rad}} + S_{\text{Rad}}) \quad (1)$$

The results presented in Table 3 are in agreement with the experimental value, $J = -351 \pm 1 \text{ (cm}^{-1}\text{)}$. It can also be remarked that the three functionals used lead to quite similar results. As shown in Figure 5(a,b), in both states, BS and HS, the spin densities

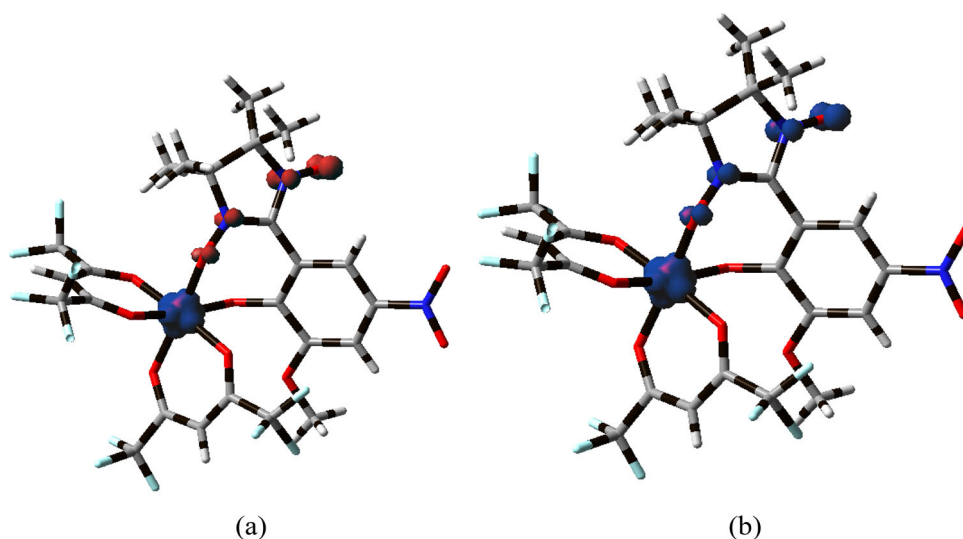


Figure 5. Spin density (0.04) isosurfaces ($0.04 \text{ e}^-/(\text{a.u.})^3$): (a) BS state; (b) HS state.

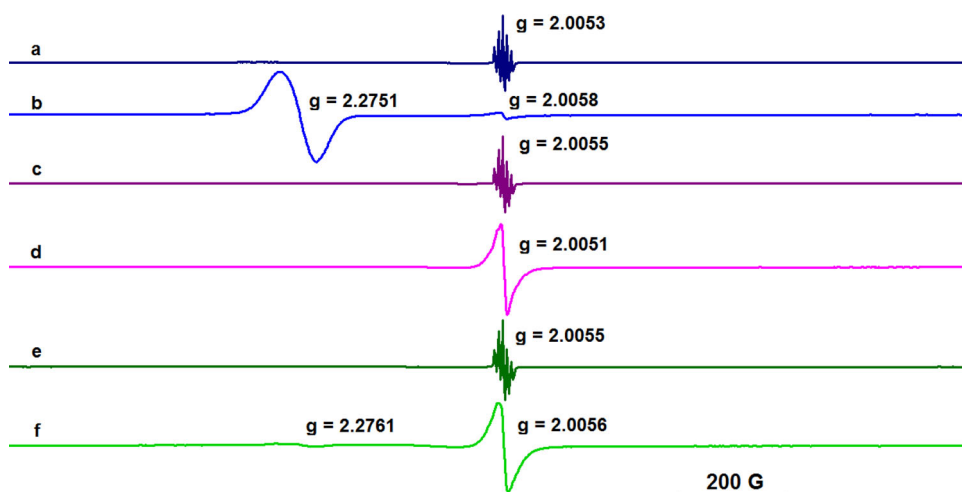


Figure 6. The EPR spectra in DCM recorded at 293 and 120 K: (a) **1** at 293 K; (b) **1** at 120 K; (c) **2** at 293 K; (d) **2** at 120 K; (e) $\text{Ni}_{0.2}\text{Zn}_{0.8}$ at 293 K; (f) $\text{Ni}_{0.2}\text{Zn}_{0.8}$ at 120 K.

are localized on the nickel ion and on the NO groups of the nitronyl-nitroxide radical, explaining the EPR spectra, *vide infra*.

3.3. EPR spectra

The EPR spectra of the three paramagnetic compounds, complexes **1** and **2** and the nitronyl-nitroxide radical, were recorded at room temperature, 293 K, and 120 K. The spectrum of HL in CH_2Cl_2 at room temperature is displayed in Figure S5 and presents the known features of nitronyl-nitroxide radicals with a g factor of 2.0053 and a five-

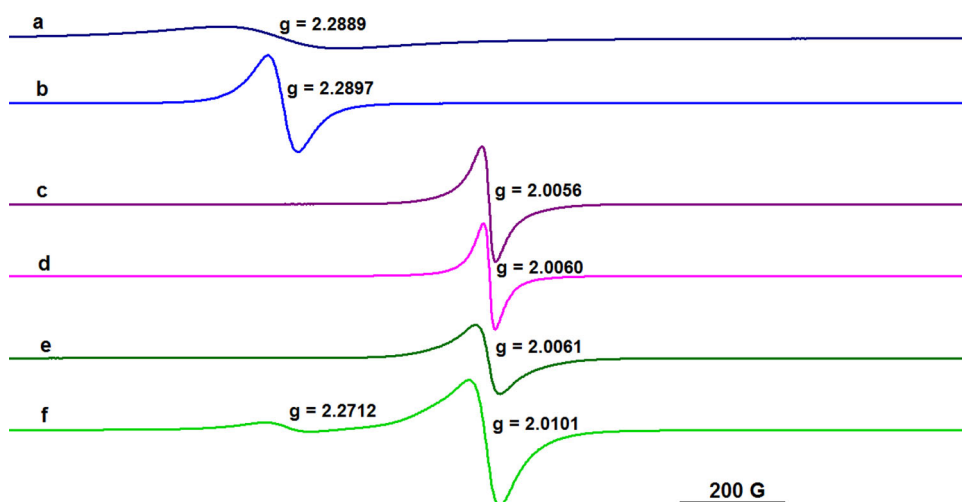


Figure 7. Solid state EPR spectra of: (a) **1** at 293 K; (b) **1** at 120 K; (c) **2** at 293 K; (d) **2** at 120 K; (e) $\text{Ni}_{0.2}\text{Zn}_{0.8}$ at 293 K; (f) $\text{Ni}_{0.2}\text{Zn}_{0.8}$ at 120 K.

Table 4. Calculated isotropic hyperfine splitting constants (G) for the three paramagnetic species optimized in DCM, using the uB3LYP functional and two basis sets, TZVP, and 6-31 g^* .

	$ a_N $ (exp)	HL		1		2	
		TZVP	6-31 g^*	TZVP	6-31 g^*	TZVP	6-31 g^*
a_{N1}	7.40	5.33	7.68	−4.98	−7.22	5.12	7.46
a_{N2}	7.55	5.06	7.59	−4.95	−7.40	5.23	7.79

line spectrum due to the hyperfine splitting (hfs) of two quasi equivalent nitrogen atoms; the values obtained by simulation are $a_{N1} = 7.40$ G and $a_{N2} = 7.55$ G. The EPR spectrum recorded at 120 K indicates a restricted motion (Figure S5c).

The EPR spectra of the two complexes and their mixture, recorded in CH_2Cl_2 , are plotted in Figure 6. At room temperature, the spectrum of the nickel complex, **1** (Figure 6(a)), presents only the signal of the organic radical ($g = 2.0053$); at 120 K, the spectrum consists of two signals, a strong one characterized by $g = 2.2751$ and a very weak signal at $g = 2.0058$; the first signal is characteristic to a paramagnetic species with the electron localized on the nickel center [20], while the weak one is due to a tiny fraction of the organic radical that can result from the dissociation of the complex in solution. As expected, at both temperatures the spectrum of **2** presents only a single signal belonging to the organic radical; the spectrum is unresolved at low temperature due to a strong broadening of the lines, but the g value is not influenced by temperature (293 K, $g = 2.0055$; 120 K, $g = 2.0051$). The isodensity spin surface displayed in Figure S6 reflects this behavior, and the spin density localized only on the NO groups. The assignment of the EPR spectra of **1** and **2** is verified by spectra e and f in Figure 6, where it can be seen that the presence of the nickel ion determines the appearance at 120 K of the very weak signal at $g = 2.2761$ previously assigned to the spin localization on nickel and a large signal at $g = 2.0056$ corresponding to **2**. The strong signal of nitronyl-nitroxide fragment observed at 120 K is due to excess of zinc complex in solution.

The same behavior is illustrated by the EPR spectra recorded in solid state (Figure 7) for **1**, **2**, and the molecular alloy $[\text{Ni}_{0.2}\text{Zn}_{0.8}]$. Although the isostructural zinc derivative, **2**, is not a diamagnetic host for **1** and cannot suppress all the dipolar interactions, some information can be extracted by comparing these spectra. At room temperature, **1** shows only a broad and weak feature at $g = 2.2889$, which is due to the $S = 1/2$ state. As expected, this signal becomes stronger at 120 K, where only the spin state $S = 1/2$ is populated (Figure 7(b)). The spectra of the zinc derivative do not change with the temperature (Figure 7(c,d)). The molecular alloy of **1** and **2** shows at room temperature (Figure 7(e)) only one signal ($g = 2.0061$) arising from **2**; at 120 K (Figure 7(f)), two signals are observed, $g = 2.0101$ (due to **2**) and $g = 2.2712$ ($S = 1/2$ ground state of **1**).

The hyperfine splitting (hfs) constants for **1** and **2** were first calculated using the same model (crystal geometry, B3LYP/TZVP) as for the magnetic data. The results listed in Table S2 show a poor agreement with the experimental ones; it is even worse with TZVP/EPR-III. A better agreement is obtained with basis set 6-31*. Therefore, all further calculations with CH_2Cl_2 as a solvent were performed using the TZVP and 6-31 g* sets (Table 4). For the three paramagnetic species, good agreement is obtained with the 6-31 g* basis, which also have the advantage of requiring short calculation times.

Conclusion

We described two new metal–radical complexes using as a ligand the nitronyl-nitroxide radical derived from *o*-vanillin. The EPR spectra of the nickel complex recorded at two different temperatures clearly show the $S = 1/2$ ground state, in line with the magnetic susceptibility measurements and theoretical calculations.

Acknowledgements

We are thankful to Anamaria Hanganu for NMR spectra recording. Also, we are grateful to Gabriel Crăciun and Adrian Apostol for EDX measurements. SC is grateful to the University of Bucharest (ICUB) for a postdoctoral fellowship.

Disclosure statement

No potential conflict of interest was reported by the authors.

ORCID

Jean-Pascal Sutter  <http://orcid.org/0000-0003-4960-0579>
Marius Andruh  <http://orcid.org/0000-0001-8224-4866>

References

- [1] (a) D. Luneau, *Eur. J. Inorg. Chem.*, **2020**, 597 (2020); (b) S. Demir, I.-R. Jeon, J.R. Long, T.D. Harris, *Coord. Chem. Rev.*, **289-290**, 149 (2015); (c) X. Meng, W. Shi, P. Cheng, *Coord. Chem. Rev.*, **378**, 134 (2019); (d) M.T. Lemaire, *Pure Appl. Chem.*, **76**, 277 (2004); (e) C. Benelli, D. Gatteschi, *Chem. Rev.*, **102**, 2369 (2002); (f) D. Luneau, P. Rey, *Coord. Chem. Rev.*, **249**, 2591 (2005); (g) A. Caneschi, D. Gatteschi, R. Sessoli, P. Rey, *Acc. Chem. Res.*, **22**, 392 (1989).

- [2] (a) J. H. Osiecki, E. F. Ullman. *J. Am. Chem. Soc.*, **90**, 1078 (1968); (b) E. F. Ullman, L. Call, J. H. Osiecki. *J. Org. Chem.*, **35**, 3623 (1970); (c) E. F. Ullman, J. H. Osiecki, D. G. B. Boocock, R. Darcy. *J. Am. Chem. Soc.*, **94**, 7049 (1972); (d) C. Hirel, K. E. Vostrikova, J. Pécaut, V. I. Ovcharenko, P. Rey. *Chem. Eur. J.*, **7**, 2007 (2001).
- [3] (a) J. Sun, Z. Sun, L. Li, J.-P. Sutter. *Inorg. Chem.*, **57**, 7507 (2018); (b) G. P. Guedes, R. G. Zorzanelli, N. M. Comerlato, N. L. Speziali, S. Santos Jr., M. G. F. Vaz. *Inorg. Chem. Commun.*, **23**, 59 (2012); (c) H. Miao, M. Li, H.-Q. Li, F.-X. Shen, Y.-Q. Zhang, X.-Y. Wang. *Dalton Trans.*, **48**, 4774 (2019); (d) Y.-F. Wang, L.-Y. Wang, L.-F. Ma. *Z. Anorg. Allg. Chem.*, **634**, 181 (2008); (e) P. Y. Chen, M. Z. Wu, T. Li, X. J. Shi, L. Tian, Z. Y. Liu. *Inorg. Chem.*, **57**, 12466 (2018); (f) P. Hu, X. Wang, Y. Ma, Q. Wang, L. Li, D. Liao. *Dalton Trans.*, **43**, 2234 (2014); (g) J. Omata, T. Ishida, D. Hashizume, F. Iwasaki, T. Nogami. *Inorg. Chem.*, **40**, 3954 (2000); (h) Z. Liu, Z. Lu, D. Zhang, Z. Jiang, L. Li, C. Liu, D. Zhu. *Inorg. Chem.*, **43**, 6620 (2004); (i) F. Furui, S. Suzuki, M. Kozaki, D. Shiomi, K. Sato, T. Takui, K. Okada, E.V. Tretyakov, S.E. Tolstikov, G.V. Romanenko, V.I. Ovcharenko. *Inorg. Chem.*, **53**, 802 (2014); (j) A. Lannes, M. Intissar, Y. Suffren, C. Reber, D. Luneau. *Inorg. Chem.*, **53**, 9548 (2014); (k) J. Guo, J. Sun, G. Sun, Z. Sun, L. Li. *Eur. J. Inorg. Chem.*, **2018**, 3241 (2018).
- [4] (a) L. B. L. Escobar, G. P. Guedes, S. Soriano, N. L. Speziali, A. K. Jordão, A. C. Cunha, V. F. Ferreira, C. Maxim, M. A. Novak, M. Andruh, M. G. F. Vaz. *Inorg. Chem.*, **53**, 7508 (2014); (b) M. Zhu, L. Li, J.-P. Sutter. *Inorg. Chem. Front.*, **3**, 994 (2016); (c) L. Xi, J. Suan, K. Wang, J. Lu, P. Jing, L. Li. *Dalton Trans.*, **49**, 1089 (2020); (d) G. Novitchi, S. Shova, Y. Lan, W. Wernsdorfer, C. Train. *Inorg. Chem.*, **55**, 12122 (2016); (e) A. A. Patrascu, S. Calancea, M. Briganti, S. Soriano, A. M. Madalan, R. A. A. Cassaro, A. Caneschi, F. Totti, M. G. F. Vaz, M. Andruh. *Chem. Commun.*, **53**, 6504 (2017); (f) A. A. Patrascu, M. Briganti, S. Soriani, S. Calancea, R. A. A. Cassaro, F. Totti, M. G. F. Vaz, M. Andruh. *Inorg. Chem.*, **58**, 13090 (2019).
- [5] M. Andruh. *Dalton Trans.*, **44**, 16633 (2015).
- [6] A. Vega, J. Padilla, M. A. Leyva, M. del Jesús Rosales, S. Bernès. *J. Mex. Chem. Soc.*, **52**, 54 (2008).
- [7] V. Ovcharenko, O. Kuznetsova, E. Fursova, G. Letyagin, G. Romanenko, A. Bogomyakov, E. Zueva. *Inorg. Chem.*, **56**, 14567 (2017).
- [8] R. Sayre. *J. Am. Chem. Soc.*, **77**, 6689 (1955).
- [9] (a) D. A. Davis, A. Hamilton, J. Yang, L. D. Cremer, D. V. Gough, S. L. Potisek, M. T. Ong, P. V. Braun, T. J. Martinez, S. R. White, J. S. Moore, N. R. Sottos. *Nature*, **459**, 68 (2009); (b) S. S. Deshpande, M. A. Jachak, S. S. Khopkar, G. S. Shankarling. *Sens. Actuators, B*, **258**, 648 (2018).
- [10] (a) G. M. Sheldrick. *Acta Crystallogr. C Struct. Chem.*, **71**, 3 (2015); (b) G. M. Sheldrick. *Acta Cryst.*, **C71**, 3 (2015).
- [11] S. Shimono, R. Tamura, N. Ikuma, T. Takimoto, N. Kawame, O. Tamada, N. Sakai, H. Matsuura, J. Yamauchi. *J. Org. Chem.*, **69**, 475 (2004).
- [12] M. J. Frisch, G. W. Trucks, H. B. Schlegel, G. E. Scuseria, M. A. Robb, J. R. Cheeseman, G. Scalmani, V. Barone, B. Mennucci, G. A. Petersson, H. Nakatsuji, M. Caricato, X. Li, H. P. Hratchian, A. F. Izmaylov, J. Bloino, G. Zheng, J. L. Sonnenberg, M. Hada, M. Ehara, K. Toyota, R. Fukuda, J. Hasegawa, M. Ishida, T. Nakajima, Y. Honda, O. Kitao, H. Nakai, T. Vreven, J. A. Montgomery, J. E. Peralta, F. Ogliaro, M. Bearpark, J. J. Heyd, E. Brothers, K. N. Kudin, V. N. Staroverov, R. Kobayashi, J. Normand, K. Raghavachari, A. Rendell, J. C. Burant, S. S. Iyengar, J. Tomasi, M. Cossi, N. Rega, J. M. Millam, M. Klene, J. E. Knox, J. B. Cross, V. Bakken, C. Adamo, J. Jaramillo, R. Gomperts, R. E. Stratmann, O. Yazyev, A. J. Austin, R. Cammi, C. Pomelli, J. W. Ochterski, R. L. Martin, K. Morokuma, V. G. Zakrzewski, G. A. Voth, P. Salvador, J. J. Dannenberg, S. Dapprich, A. D. Daniels, O. Farkas, J. B. Foresman, J. V. Ortiz, J. Cioslowski, D. J. Fox. *GAUSSIAN 09, Revision C.01*, Gaussian, Inc., Wallingford, CT (2009).
- [13] F. Weigend, R. Ahlrichs. *Phys. Chem. Chem. Phys.*, **7**, 3297 (2005).
- [14] A. D. Becke. *J. Chem. Phys.*, **98**, 5648 (1993).
- [15] Y. Wang, J. P. Perdew. *Phys. Rev. B*, **44**, 13298 (1991).

- [16] (a) R. Valero, R. Costa, I. de P R Moreira, D. G. Truhlar, F. Illas. *J. Chem. Phys.*, **128**, 114103(2008).
- [17] (a) L. Hermosilla, J. M. Garcia de la Vega, C. Sieiro, P. Calle. *J. Chem. Theory Comput.*, **7**, 169 (2011); (b) L. Hermosilla, P. Calle, J. M. G. de la Vega, C. Sieiro. *J. Phys. Chem. A*, **110**, 13600 (2006);(c) A. Tanaka, K. Nakashima. *Magn. Reson. Chem.*, **49**, 603 (2011);(d) C. Zhao, R. Dao, Y. Wang, J. Yao, H. Li. *Chem. Phys.*, **517**, 13 (2019);(e) L. Hermosilla, P. Calle, J. M. García de la Vega. *RSC Adv.*, **5**, 62551 (2015);(f) O. I. Gromov, S. V. Kuzin, E. N. Golubeva. *J. Mol. Model.*, **25**, 93 (2019).
- [18] C. Stroh, E. Belorizky, P. Turek, H. Bolvin, R. Ziessel. *Inorg. Chem.*, **42**, 2938 (2003).
- [19] E. Ruiz, J. Cano, S. Alvarez, P. Alemany. *J. Comput. Chem.*, **20**, 1391(1999).
- [20] (a) Z.-H. Zhang, S.-Y. Wu, P. Xu, L.-L. Li. *Braz. J. Phys.*, **40**, 361 (2010); (b) R. Srinivasan, I. Sougandi, R. Venkatesan, P. S. Rao. *Proc. Indian Acad. Sci. (Chem. Sci.)*, **115**, 91 (2003).